Drop entrainment from the surface of oil mist filters: mechanisms, kinetics, and drop spectra

S. Wurster, H.E. Kolb, J. Meyer and G. Kasper
Institut für Mechanische Verfahrenstechnik und Mechanik,
Karlsruher Institute für Technologie (KIT), 76131 Karlsruhe, Germany

ABSTRACT

Oil entrainment from coalescence filters has been characterized by different techniques. Drop spectra and entrainment rates were measured by a combination of techniques from <1 µm up to >1 mm over long periods of time. Dominant entrainment mechanism(s) are identified on the basis of comparisons of entrainment rates measured in different regions of the filter surface with rates of air bubble formation, measurements of oil film thickness, as well as visual observations. Experiments are supported by force estimates to entrain oil into the gas flow.

KEYWORDS

Air filtration, oil mist, liquid entrainment, blow-off, optical size analysis

Introduction

Submicron oil mist is generated in large amounts by various processes of industrial relevance, such as in the crankcases of combustion engines, by oil-lubricated air compressors, during metal cutting, and during natural gas processing and transport. Oil aerosols are effectively removed by fibrous filters which operate in steady state for most of their useful life, i.e. deposited and coalesced oil must drain continually under the influence of gravity. At the same time, the air flowing through the filter maintains a flow of coalesced oil toward the back of the filter and may cause some of that liquid to become (re)-entrained ("blown off") as a secondary aerosol (e.g. Raynor and Leith, 2000). Not enough is known currently about this latter mechanism to provide reliable guidance for filter optimization.

Earlier studies of oil transport inside such filters (Kampa et al., 2014) had shown that oil drains from the surface of the media in the form of isolated droplets or as a quasi-continuous film, depending on whether the media are wettable to oil or not (Fig. 1). Based on these observations one would assume that entirely different entrainment mechanisms are at work, namely blow-off of rather large drops in case of non-wettable filters, vs. bubble

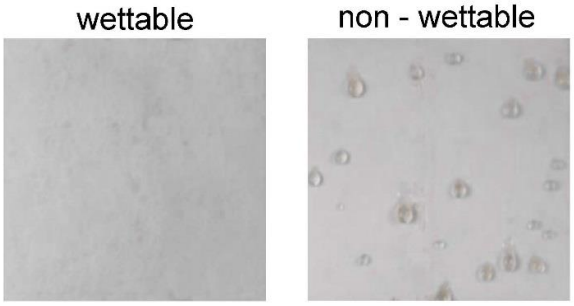

Fig. 1 - *Visualized oil drainage on wettable (left) and non-wettable (right) filter media.*

bursting (accompanied by the formation of secondary drops) in the oil film of wettable filters (Mullins et al., 2014).

This hypothesis was tested experimentally for glass microfiber media under typical operating conditions of compressed air filtration (filtration velocities <1 $m \cdot s^{-1}$) by comparing entrainment rates with visual observations of drop blow-off and bubble formation rates. A combination of measurement techniques was used to capture the complete blow-off spectrum, including especially the in-situ detection of large drops up to >1 mm. Entrainment rates were measured for a range of filter operating parameters including filtration velocity and oil loading rate. These data are compared with estimates of forces required to cause bubble formation vs. blow-off.

Experimental techniques used

The wide spectrum of possible drop sizes generated by entrainment was covered by 4 different techniques, two for the combined submicron and micron range below about 10 µm, and two for the larger drops up to several millimeters in diameter. For practical reasons the respective devices were integrated into separate setups as shown in Fig. 2 (a) and (b).

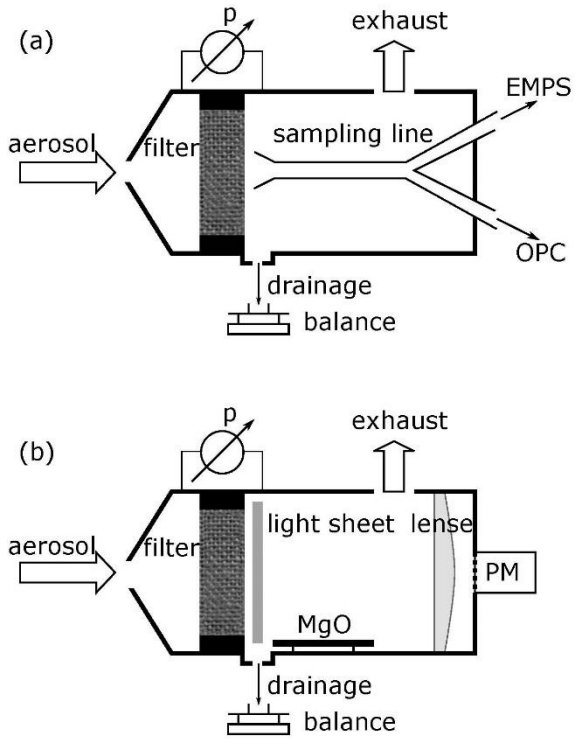

Fig. 2 - *Schematic diagrams of the setups to measure entrainment drop size spectra, concentrations and rates.*
(a): Setup for drops ranging from 0.01 to 10 µm by optical particle counter (OPC) and/or electrical mobility particle sizer (EMPS).
(b): Setup for drops ranging from 10 µm to about 2 mm by impaction on MgO coated glass plates and a custom-build large drop detection system (LDDS). Differential pressure across the filter and drained oil mass were recorded in both setups.

An ***electrical mobility particle sizer (EMPS)*** was used to cover the size range from about 0.01 to 0.7 µm at a sample flow rate of ca. 1 l min^{-1}. This device combines an aerosol neutralizer (a 20 mCi Kr^{85} source), a DMA (Knutson and Whitby, 1975) and a condensation particle counter (TSI, Model 3022). Since the size range below 1 µm overlaps with the primary aerosol used to load the filter, measurements were done

intermittently by switching from aerosol to a clean gas flow. After 2 minutes of system purging a 5-min. scan followed. Although these measurements are not strictly continuously, results are representative since the oil distribution within the filter does not change substantially in the time scale of a few minutes (Kampa et al., 2015).

An ***optical particle counter (OPC)*** of in-house design was used to cover the size range between 0.5 to 10 µm with 150 size classes. Its operating principle is based on counting and sizing via light scattering on single particles (Keusen, 2003; Heim et al., 2008; Umhauer et al., 2008). The device was operated continuously throughout an experiment and provided one data point per minute. A rectilinear flow path between the rear of filter and OPC inlet ensures a certain degree of isokineticity. Thus in first experiments the sampling line was centered on the filter element. To resolve spatial entrainment rates with the OPC by maintaining isokineticity further precautions were necessary. The filter chamber was split into two hales. One halve, which contains the sampling line was slightly enlarged and mounted opposite to the filter as shown in Fig. 3. Due to adjustable mounting of one chamber halve along the vertical the sampling line was always kept rectilinear between filter and OPC inlet to prevent losses of large drops.

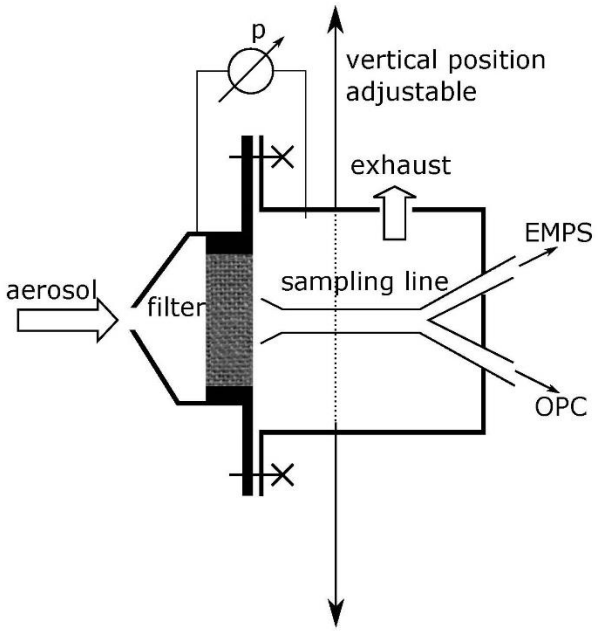

Fig. 3 - *Schematic diagram of the modified setup to measure entrainment drop size spectra, concentrations and rates for submicron and micron drops by optical particle counter (OPC) and/or electrical mobility particle sizer (EMPS). The chamber halve, which contains the sampling line is adjustable in its vertical position thus resolving entrainment along the direction of gravity.*

The size range between about 10 and 200 µm could not be covered by any readily accessible real-time measurement technique. Thus an off-line method described originally by May (1950) to count and size airborne droplets was used. Glass slides (10 cm x 10 cm) coated with a thin layer (thickness larger than drop size) of magnesium oxide collect impacting droplets. Resulting circular caters are determined by scanning the plate surfaces with an incident light microscope. Crater diameters generated with monodisperse oil droplets of known sizes were approximately 1.3 times larger than original droplet diameters. Although the ***magnesium oxide (MgO) technique*** does not include drops which miss the glass plate and misleads the counted number in case

of overlapping droplets, this approach provides some valuable data on the size spectrum difficult to measure with conventional techniques.

For drops larger than about 100 µm up to several millimeters a dedicated measurement system for continuous sizing and counting was developed. These large drops contribute most to mass entrainment and thus are of particular interest (Kampa et al., 2011; Wurster et al., 2012). Since droplets in this size range settle very rapidly and would also impact immediately at each deflection, it is necessary to detect and size them in-situ immediately behind the filter. A schematic operating principle of the custom-build ***large drop detection system (LDDS)*** is shown in Fig. 4. The light sheet technique is based on the expansion of a continuous wave laser beam into a thin sheet of light parallel to the back of the filter. Entrained droplets crossing this sheet generate pulses of scattered light which are detected by a photomultiplier, stored with time stamp and classified according to pulse height. This permits the recording of entrainment time series over many hours.

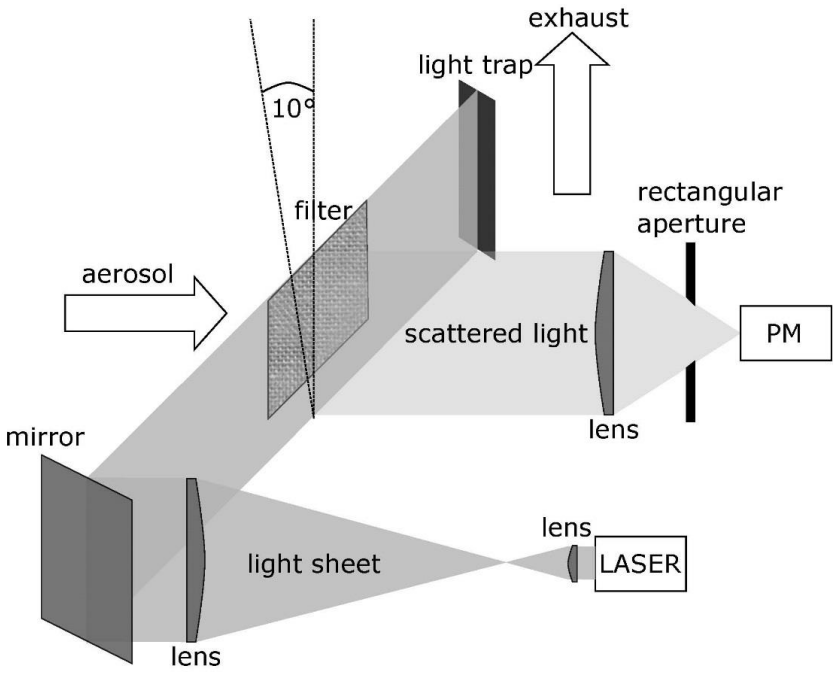

Fig. 4 - *Schematic principle of Large Drop Detection System (LDDS): Light scattered perpendicular to the light sheet is detected by a photomultiplier (PM) tube and classified according to its height into drop size. By expansion of laser light into one direction about a factor of 200, a light sheet is generated. A plane with 8 cm in height is channeled by a mirror parallel, at a 5-mm distance, to the rear face of the filter media. The device is tilted 10° against the vertical to ensure that all drops, even those which translate predominantly into the direction of gravity, are captured by the LDDS.*

Entrained drops whose trajectories are predominantly gravity driven and thus settle downwards a few mm behind the filter face are difficult to detect. Thus, to capture these particles the filter dimensions (50 mm x 50 mm) as well as the distance between filter and light sheet (5 mm) are chosen in a way that for a device tilt of 10° against the horizontal all drop trajectories cross the measurement volume. Effective gravitational forces differ less than 2 % with a 10° tilt.

Entrainment size spectra

A typical example of entrainment size spectra for wettable and non-wettable glass fiber type filters is given in Fig. 5. While submicron drops contribute insignificantly to entrainment, both types of coalescence filter media exhibit two distinct peaks in the mass spectra, one narrow peak in the vicinity of a few µm and another, rather broad one in the range of several 100 µm as seen in Fig. 5.

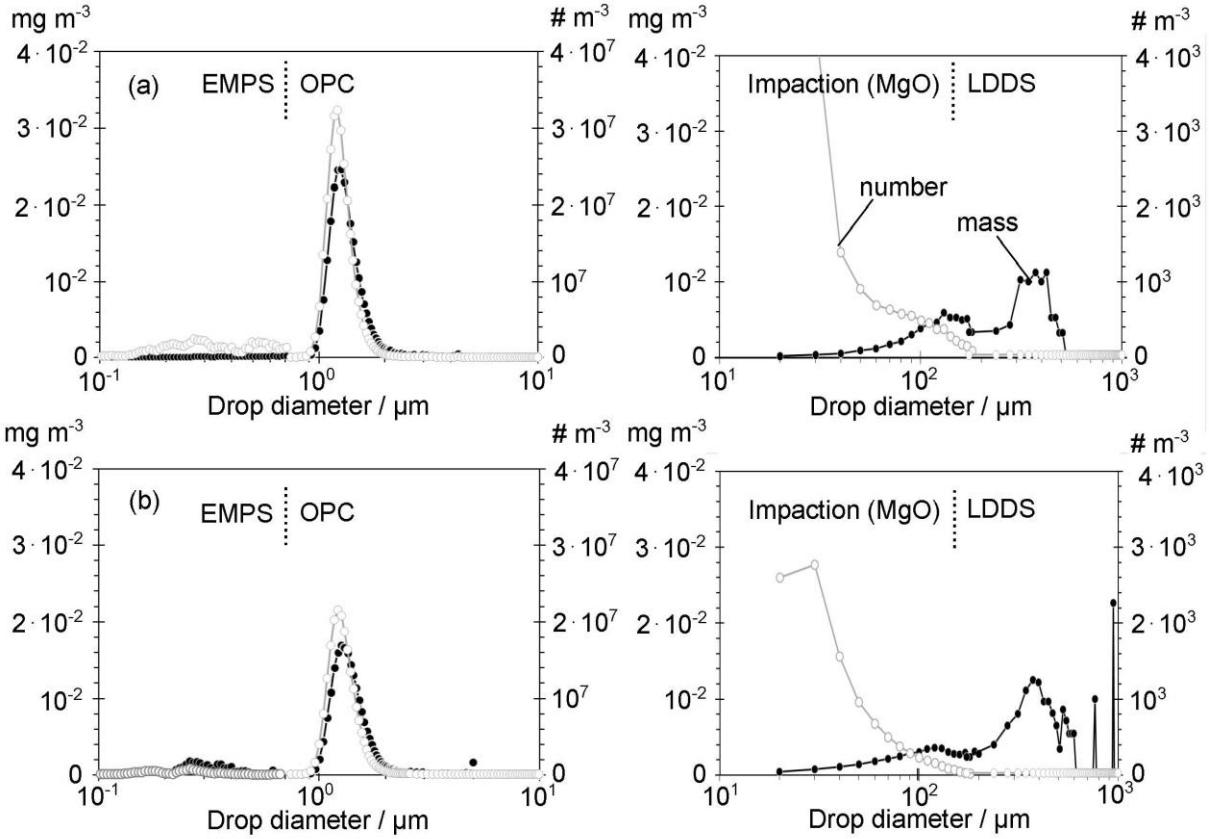

Fig. 5 - *Entrainment spectra from 5 layers of wettable (a) and from 5 layers of non-wettable (b) glass fiber filter media, loaded with ca. 0.45 g·m^{-3} at 25 cm·s^{-1} entry velocity; combined use of EMPS (up to 0.7 µm), OPC (ca. 0.5 - 10 µm), impaction technique by May (>10 µm) and custom-build light sheet technique (150 - 2500 µm).*

Aerosols generated by bursting air bubbles have been investigated extensively for water and aqueous salt solutions (e.g. Cipriano and Blanchard, 1981; Resch et al., 1986; Blanchard and Syzdek, 1988) and it is well known that this mechanism can also lead to the formation of multimodal spectra including large drops (Garner et al., 1954; Newitt et al., 1954). Such large drops (>100 µm) are visually observed at oil mist filters, too. In case of liquid shear off, the resulting size spectra may also be bimodal since large drops are often accompanied by smaller satellite drops (Ambravaneswaran et al., 2004). The formation of satellite drops depends on the ratio of viscosity and surface tension forces (Stone, 1994). Thus spectra are insufficient to curtail predominant entrainment mechanism.

Entrainment rates

Real-time optical techniques, such as OPC and LDDS, provide time resolved data on drop generation and thus on the entrainment rate. Sample data for glass fiber filters are shown in Fig. 6 for initially dry media. The measurements were taken with a time resolution of 1 min. The results obtained by OPC (for small drops) are shown in the left hand graphs, and these obtained by LDDS in the right graphs (for large drops). Also included in each graph are the corresponding curves of differential pressure.

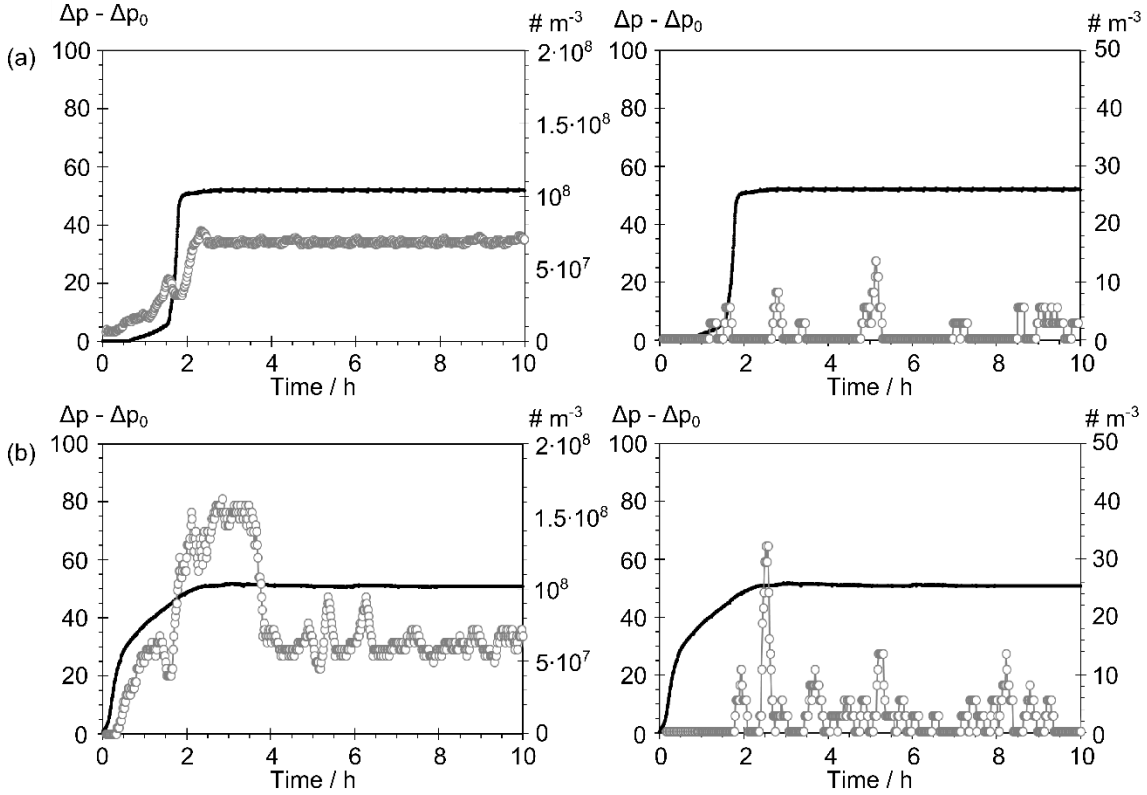

Fig. 6 - *Number based entrainment rates vs. time for a wettable (a) and non - wettable (b) glass fiber medium, recorded at 1-min. intervals by OPC (left) and by LDDS (right). Entrainment rates are shown in gray, differential pressure curves are shown in black. The loading rate was ca. 0.45 g·m^{-3}, the filter face velocity was 25 cm·s^{-1}.*

The Δp evolution is typical for glass fiber type media (Kampa et al., 2015), with a steep initial rise due to accumulating oil followed by a leveling-off once steady state is reached. Entrainment starts to kick in, shortly before the Δp curve levels off, at the point in time corresponding to the begin of oil drainage on rear face of filter media (Kampa et al., 2014).

In steady state, the concentration of generated micron sized drops in the OPC range is quite significant at >10^7 per m^3, while large drops are emitted by the filter surface at a rate of roughly one per minute. A method described by Preining (1983) was applied to the LDDS data to estimate the degree of randomness of these rare events. It was found that these large drops are blown-off in groups, regardless of filter wettability,

followed by periods of relative inactivity (Wurster et al., 2015a). This was a first indication that bubble bursting may play an important role for entrainment.

Bubbling vs. blow-off

Based on the hypothesis of drop detachment ("blow-off") as the predominant entrainment mechanism for non-wettable filters, one would expect a distinct correlation between the momentary entrainment rate and the number of drops visible on the downstream face of such a medium. Fig. 7 shows a series of photographs taken at certain points in time during filtration, beginning with initially dry filters. Starting from the completely dry filter, the number of drops visible on the filter increases noticeably during the first 3 h, as more and more oil channels propagate to the back and form drops. With time, more and more drops run-off ("drain") when exceeding a critical drop size (~ 5.5 - 6 mm). The number of visible drops peaks around 3 h from the beginning of operation but then surprisingly decreases again and goes to zero in the later stages of filtration. Experiments with oil containing fluorescing dye showed that draining drops leave a tiny trace of oil on the filter surface, thus subsequent oil exiting downstream forms either no drops or much smaller ones running off sooner. An example of tiny oil traces left behind is shown in Fig. 8.

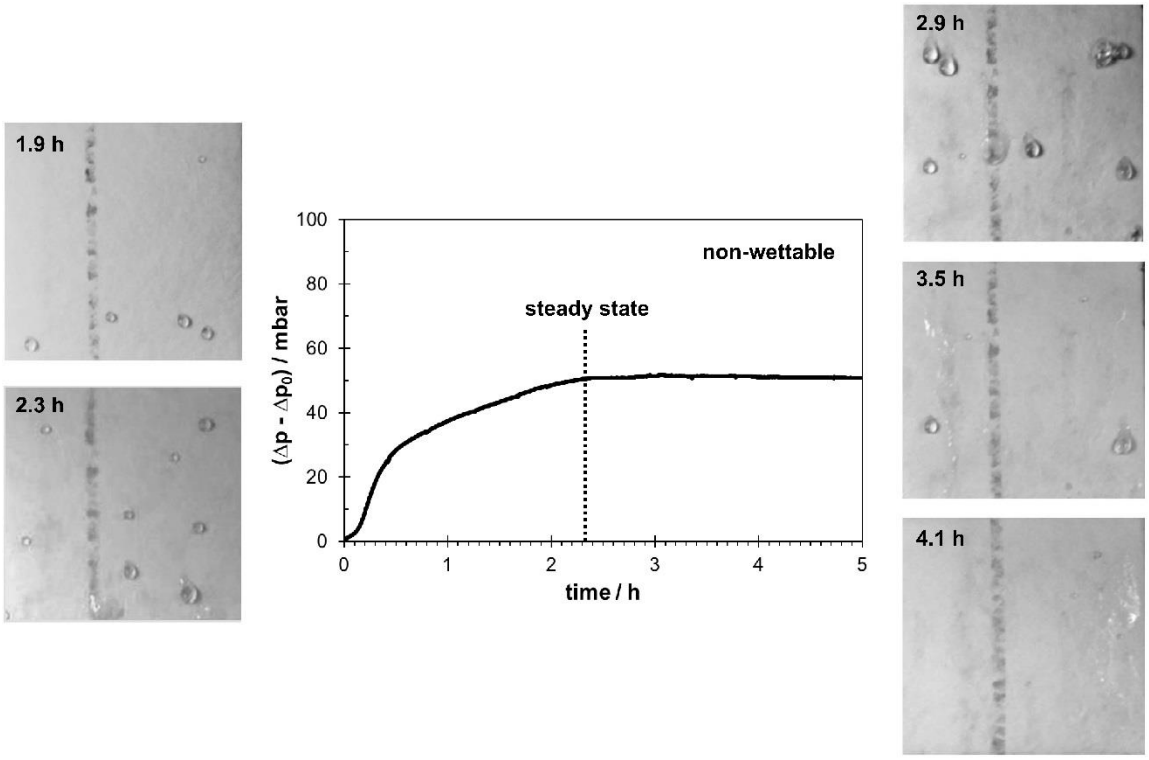

Fig. 7 - *Drops entering downstream and draining from non-wettable glass fiber type filter during mist filtration in correlation with corresponding pressure drop across filter medium; two images on the left are taken before quasi steady-state filtration conditions are reached, three images on the right are taken at constant Δp from 5 cm x 5 cm filter face.*

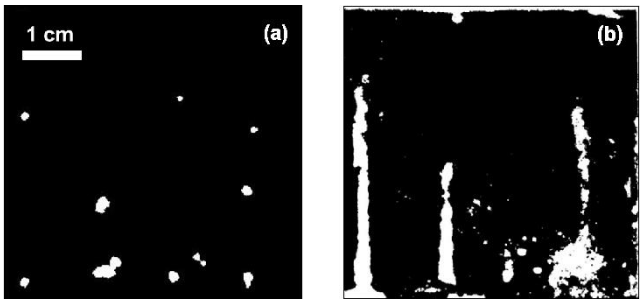

Fig. 8 - *Images obtained with fluorescent oil after illumination with UV light and graphical analysis. In (a) first exiting oil drops are displayed as white dots. Draining oil drops in (b) leave an oily trace (white pixels) on its way downwards into the direction of gravity.*

Fig. 9 compares momentary entrainment per 1 min intervals and the momentary number of visible drops (in 5 min intervals) across the entire filter face of a non-wettable glass fiber filter. There is a good agreement between the onset of entrainment and first drops formed. The peak number of drops present on the filter surface coincides with an initial burst of entrainment. Without the presence of visible drops on the filter face the entrainment concentration levels off and remains on a rather lower, but constant level. When microfilms of draining oil cover most of the surface, the situation is quite similar to the wettable case. Since much more large drops are counted than observed on filter surface, another hint on bubbling as the predominant mechanism is given.

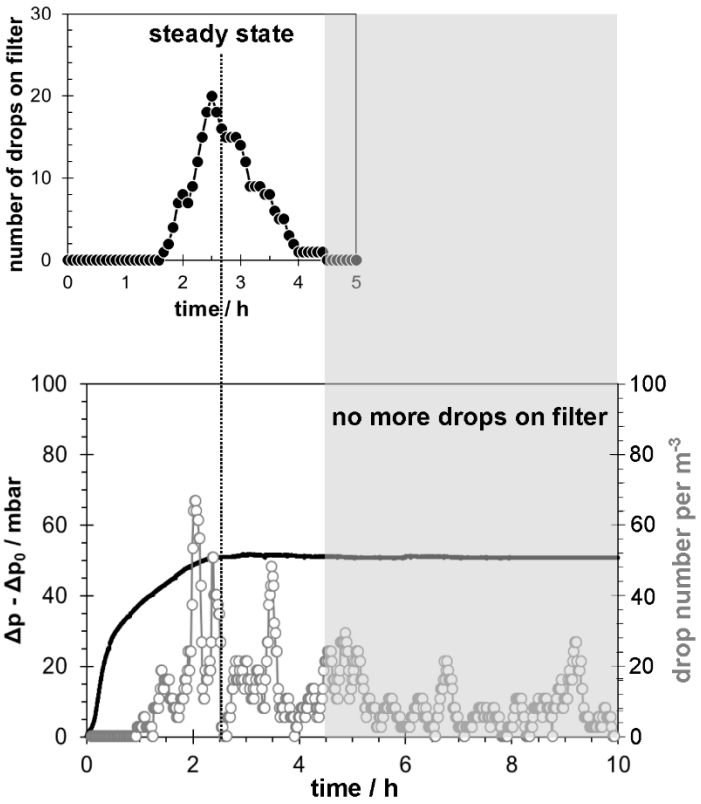

Fig. 9 - *Number of drops present on non-wettable filter, counted in 5 min. intervals and momentary entrainment concentration for the same type of glass fiber filter, loaded with 0.45 g·m^{-3} and face velocity of 25 cm·s^{-1}.*

For the entrainment burst (when visible individual drops adhere on filter surface) the likelihood of blow-off has been compared to run-off (Wurster et al., 2015b) on the basis of a force balance similar to the Weber number. It was found that even large oil drops are unlikely to get blown off at typical air flow velocities of 1 m·s^{-1} or less, and thus tend to drain.

The required force to form and burst a bubble was estimated on the basis of the capillary pressure inside a bubble. Typical bubble sizes were determined from images taken with a high speed camera. It was found that the most frequent diameter of the bubble cap before bursting was about 1 - 1.5 mm for both wettable and non-wettable

filters. The required force, obtained as the product of capillary pressure times peak bubble area, was thus much smaller than for blow-off. Reported detachment forces for a variety of drop sizes measured with atomic force microscope (Mullins et al., 2005 and 2007; Dawar et al., 2010; Hotz et al., 2015) are also about an order of magnitude larger than for bubble formation. Thus, bubbling appears to be the preferred mechanism for entrainment.

Figs. 10 to 12 show the dependence of entrainment on filter face velocity and oil loading rate. Entrainment is expressed both as rate and as entrained oil concentration. The data points were obtained with LDDS (Figs. 10 and 11) and OPC (Fig. 12) and each represent an average over an extended period of filter operation in steady state. For non-wettable filter media the average entrainment rate may include a part of the burst.

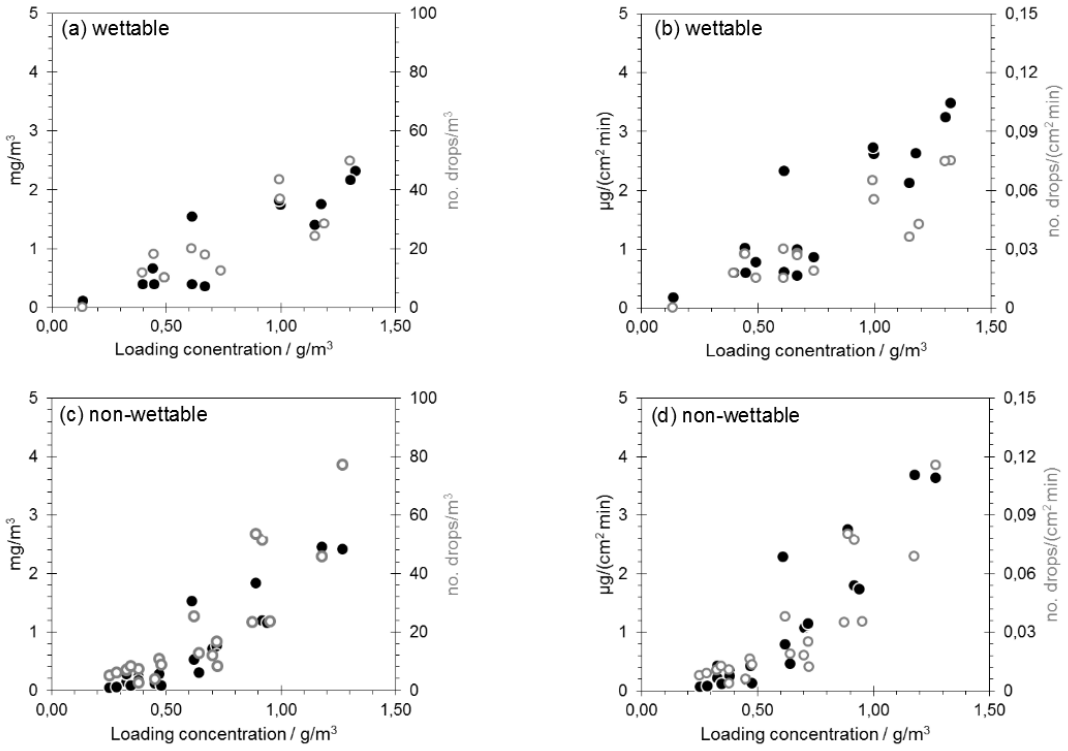

Fig. 10 - *Entrained oil concentrations (left) and rates (right) for large drops* ***as a function of oil load*** *at 25 cm·s^{-1} face velocity for wettable (top) and non-wettable (bottom) glass fiber media. Number (open symbols) and mass (solid symbols) based concentrations and rates are included in each diagram.*

The oil delivery rate, i.e. the product of inlet aerosol concentration c, face velocity v and filter cross section A_{filter}, was varied by about a factor of 5 at a fixed filtration face velocity of 25 cm·s^{-1}. The data show a much more pronounced influence of the loading rate than of the face velocity. Thus it is the magnitude of oil reservoir (either drops or films) that matters predominantly for entrainment, not the flow velocity. These trends and dependencies for entrainment of large drops are mirrored in the data for micron sizes drops, measured with the OPC and is consistent with other results showing that blow-off is not the dominant mechanism.

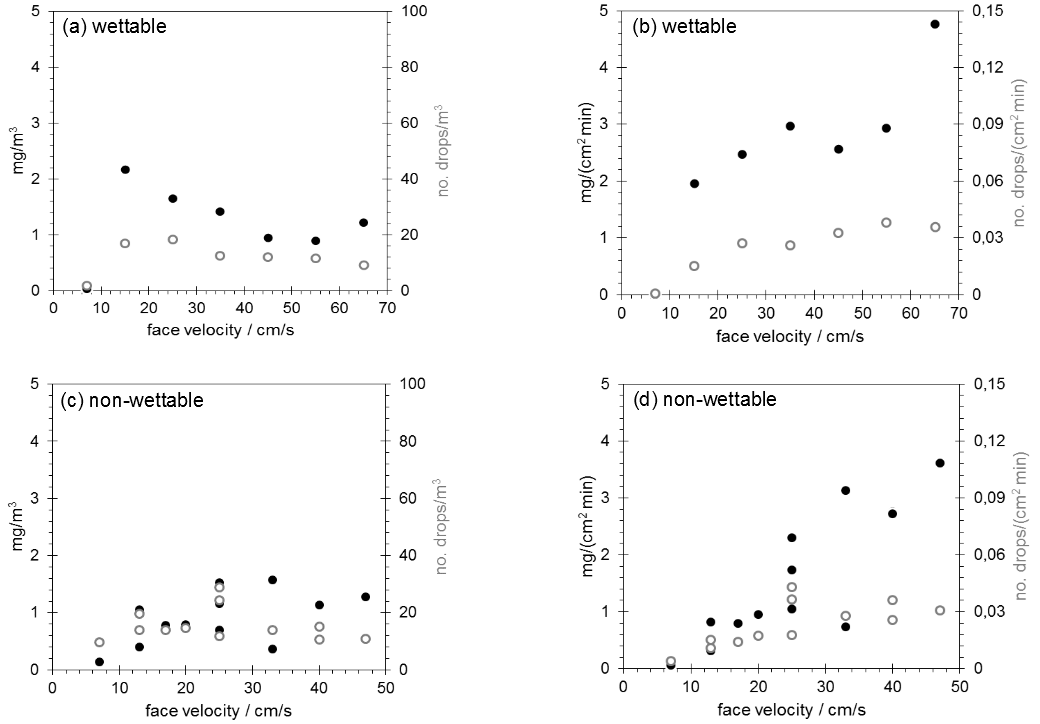

Fig. 11 - *Entrained oil concentrations (left) and rates (right) for large drops* ***as function of face velocity*** *at respective oil loading rates ($c \cdot v \cdot A_{filter}$) of 0.7 $g \cdot h^{-1}$ and 0.5 $g \cdot h^{-1}$ for wettable (top) and non-wettable (bottom) glass fiber media. Number (open symbols) and mass (solid symbols) based concentrations and rates are included in each diagram.*

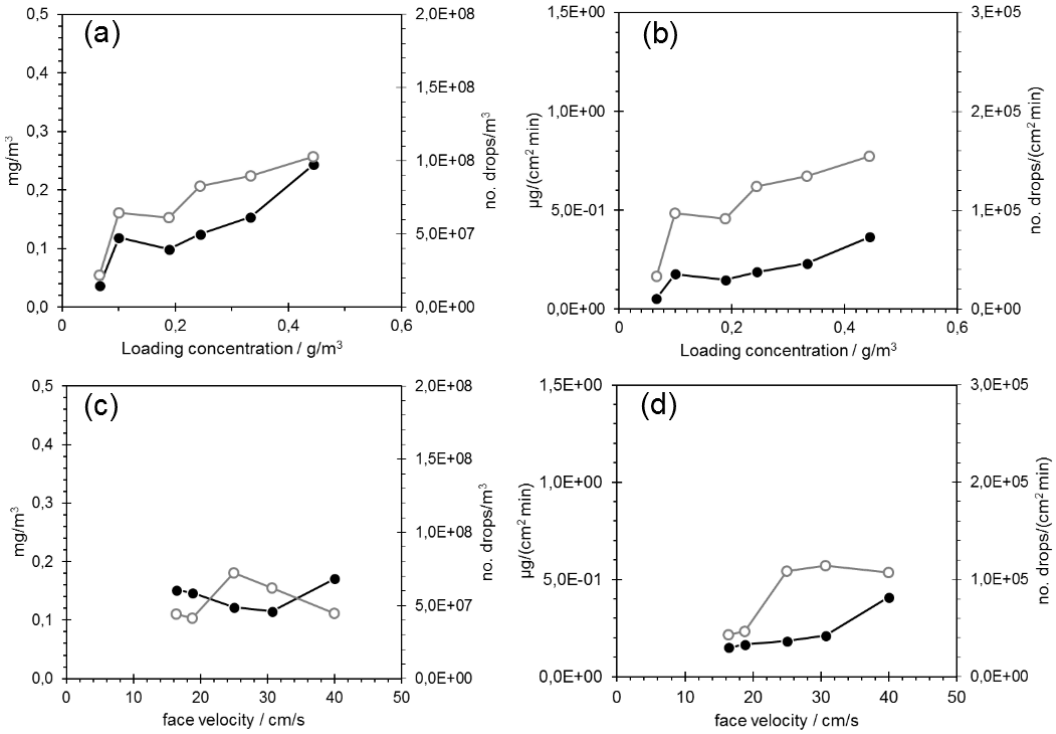

Fig. 12 - *Entrainment concentrations (left) and rates (right) of micron sized drops as function of oil loading concentration at 25 cm s^{-1} (a, b) and of face velocity at loading rate of 0.8 $g \cdot h^{-1}$ (c, d) for wettable glass fiber media. Number (open symbols) and mass (solid symbols) based concentrations and rates are included in each diagram. The OPC did not sample from the entire filter surface, but from a circular region of about 2 cm^2 at the center of the filter.*

Entrainment rate as function of position in vertically installed filter media

Many mist filters are installed in vertical orientation, with a downward directed drainage of oil along the filter surface in the form of a surface film. Since oil exits uniformly across the surface of glass fiber media through oil channels (Kampa et al., 2014), the thickness of the drainage film must increase toward the bottom of the filter during stead-state operation. For a multi-layer wettable filter, the effective thickness of this film (i.e. assuming a uniform oil layer in horizontal direction) was determined from measurements at different levels, based on the difference in saturation between the last layer (which contains the drainage oil layer) and previous layers (Fig. 13).

A comparison of film thickness data with measurements of the entrainment rate by OPC at different vertical positions on the filter surface is shown in Fig. 13 for one set of operating conditions. The variation in film thickness from top to bottom correlates quite well with the entrainment rate.

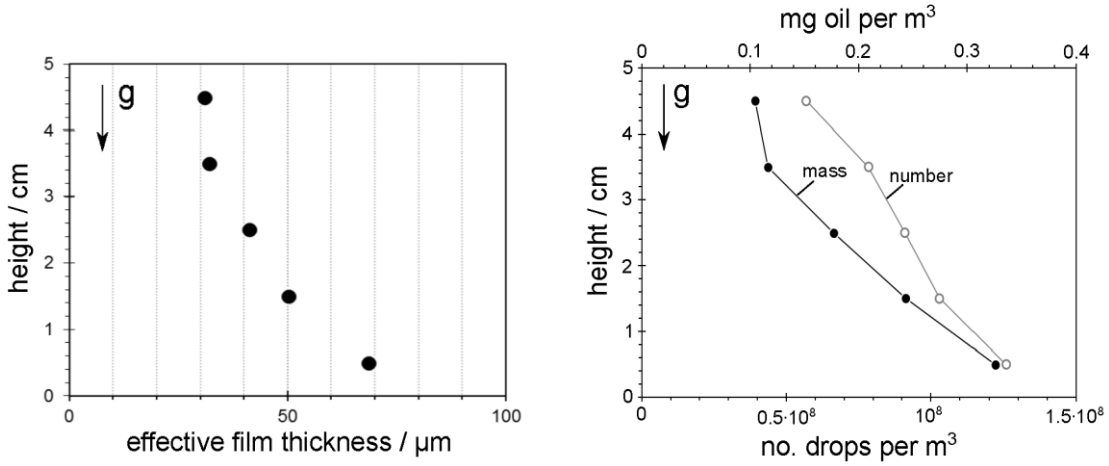

Fig. 13 - *Left: Average film thickness vs. height in vertical direction from top to bottom for a 5 cm x 5 cm filter sample. Right: Entrained drop concentrations measured with OPC at 25 cm·s^{-1} face velocity and aerosol load concentration of 1 g·m^{-3}, expressed as number (open symbols) and mass (solid symbols) concentration.*

Entrainment rates vs. rates of bubble formation on the filter surface

Although visual observations as well as quantitative data point to bubbling as the prevailing entrainment mechanism, there is still a lack of direct experimental evidence because the rate of bubble formation on the surface of a filter has never been measured and its dependence on operating parameters is not known. (Film thickness seems to play a role, as we have seen.) Therefore an experiment was set up, as shown in Fig. 14, to detect and count bursting bubbles at different points across the surface of a glass fiber filter. Basically the filter surface was scanned either in vertical or in horizontal direction by a movable high-speed camera with a field of view of 6 mm x 6 mm. The necessary illumination to take images at a rate of 500 frames per second was provided by two light sources placed roughly at a 45° angle on either side of the optical axis. Although oil/air bubbles are not directly visible due to a lack of contrast between clear oil and a white filter surface, one can detect the glare points

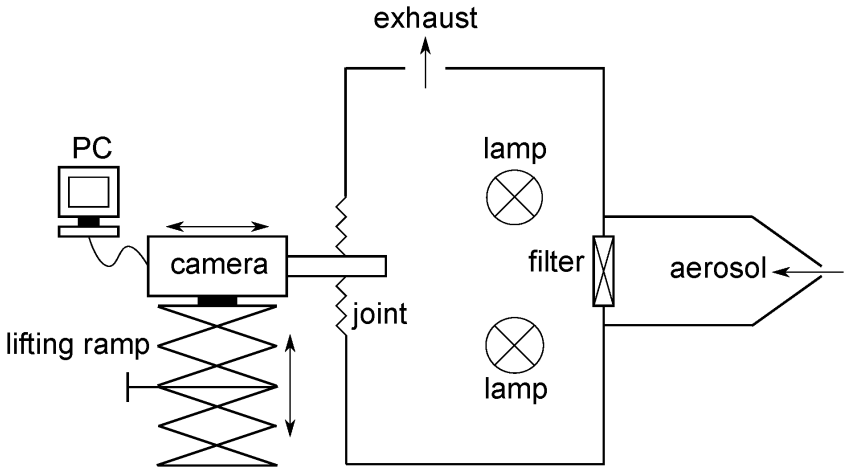

Fig. 14 - *Setup to count bubbling rates from glass fiber filters by scanning of filter surface with high-speed camera which is moveable in all three spatial directions.*

from the light sources. In this way bubbles were detected and counted frame by frame with the help of a custom analysis routine that monitors the appearance and disappearance of glare points, thereby indicating the location of bubbles and the moment when a bubble bursts. The method provides consistent data, but the absolute rate currently has an uncertainty on the order of a factor of at least 1.5. The camera memory limits measurement sequences to 4 s each between read-outs, and each repositioning of the camera also takes a few minutes, but one can use the technique to obtain steady-state bubbling rates at intervals of 15 minutes between measurements.

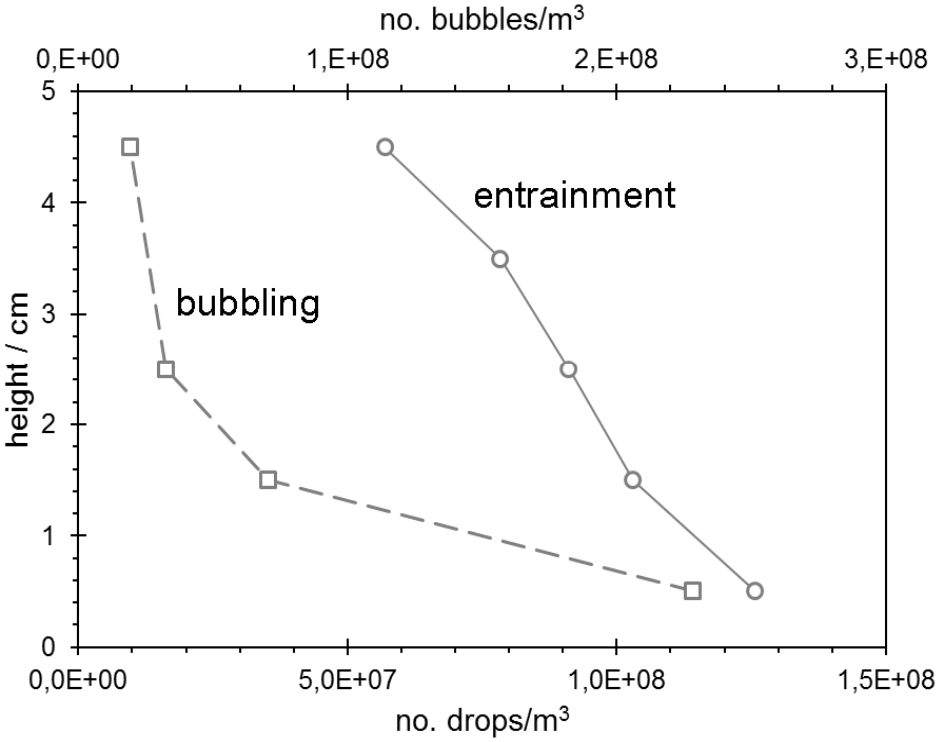

Fig. 15 - *Comparison of entrainment rates and bubble formation rates as a function of vertical position on the filter surface (v = 25 cm·s^{-1}, aerosol load concentration of 1 g·m^{-3}).*

Fig. 15 shows the bubble formation rate measured in this way at different vertical positions along the filter surface and compares it with the entrainment rates measured by OPC at the same location. (Note that time is expressed in terms of the volume of air passing through the filter.) Apparently there is a good qualitative correspondence between the two quantities, although the trends are somewhat different. The increase in entrainment rate is roughly linear from top to bottom, whereas the bubble formation rate has an exponential tendency. A quantitative analysis would require more data and a more detailed understanding of the relationship between bubble formation and film thickness, which is currently being studied.

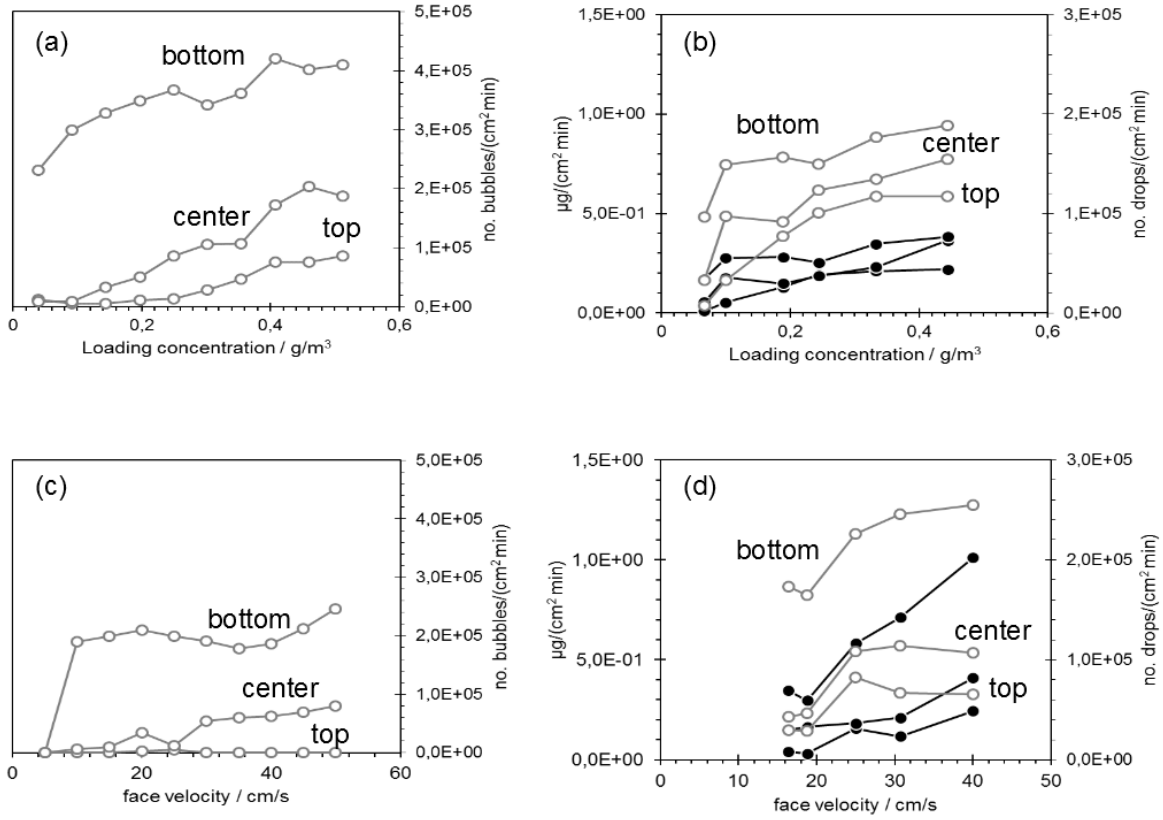

Fig. 16 - *Bubbling rates (LEFT) and entrainment rates (RIGHT) as function of aerosol load concentration at constant v = 25 cm·s^{-1} (TOP) and function of face velocity at constant loading rates of 0.8 g·h^{-1} (0.35 g m^{-3}) and 1 g·h^{-1} (0.45 g m^{-3}) (BOTTOM). Number (open symbols) and mass (solid symbols) based rates are included for entrainment data. Bubbling rates are number based. Entrainment rates are measured by OPC.*

Fig. 16 compares the same type of data as a function of oil loading rate at a fixed face velocity of 25 cm·s^{-1} (graphs a and b at top), and as a function of face velocity at a fixed oil load of 0.8 and 1 g·m^{-3}, respectively (graphs c and d at bottom). Bubbling rates are averaged each across a horizontal strip of the filter face. One notices the similarity in behavior, with both rates increasing from top to bottom, and a much stronger dependence on the loading rate than on the air velocity. These trends are the same regardless of vertical position on the filter surface.

Summary

A measurement concept to detect entrainment drop spectra ranging from nanometer up to millimeter is presented and used to determine time dependent entrainment rates on a number and mass basis. A light sheet technique with optically defined measurement volume, which allows the detection of large, sub-millimeter sized drops blown off from filter, was developed. Entrainment spectra are at least bimodal with two distinct mass peaks, one in the low (above ca. 1 µm) and a second one in the high micron (above ca. 100 µm) range. An entrainment “burst” was found to occur on non-wettable filters only, when starting filtration with initially dry media.
A technique was developed and applied also to measure the rate of formation and bursting of air bubbles on the filter surface. Furthermore, the thickness of the drainage film on the rear face of the filter was measured as a function of vertical position. All observations and quantitative data point to bubbling (and bubble collapse) as the dominant mechanism of entrainment for glass fiber type filters operated in the range below 1 $m \cdot s^{-1}$. Bubbling is correlated with the local thickness of the oil film. Entrainment and bubble formation rate are strongly dependent on the oil loading rate of the filter, but weakly dependent on the filtration velocity.

Acknowledgments

The authors gratefully acknowledge funding from the German Research Foundation DFG (Grant KA 1373/22), as well as Atlas Copco Airpower NV and MANN+HUMMEL GmbH for their longstanding support of the project.

References

Ambravaneswaran, B., Subramani, H. J., Phillips, S. D. and Basaran, O. A., 2004. Dripping-jetting transitions in a dripping faucet. Phys. Rev. Lett. 93 (3):034501.

Blanchard D.C. and Syzdek L. D., 1988. Film Drop Production as a Function of Bubble Size. J. Geophys. Res. 93, 3649.

Cipriano R. J. and Blanchard D.C., 1981. Bubble and Aerosol Spectra produced by a laboratory “breaking wave”. J. Geophys. Res. 86, 8085.

Dawar, S. and Chase, G. G., 2010. Correlations for transverse motion of liquid drops on fibers, Sep. Purif. Technol., 72, 282-287.

Garner, F. H., 1954. The size distribution and entrainment of droplets. Trans. Instn Chem. Engrs. 32, 222-235.

Heim, M., Mullins, B. J., Umhauer, H., Kasper, G., 2008. Performance evaluation of three optical particle counters with an efficient “multimodal” calibration method. J. Aerosol Sci. 39, 1019-1031.

Hotz, C. J., Mead-Hunter, R., Becker, T., King, A. J. C., Wurster, S. and Kasper, G., 2015. Detachment of droplets from cylinders in flow using an experimental analogue, J. Fluid Mech., 771, 327-340.

Kampa D., Buzengeiger J., Meyer J., Mullins B. and Kasper G., 2011. Temporal evolution of the saturation profile of an oil-mist filter. FILTECH 2011, Wiesbaden, II-233 - 240.

Kampa, D., Wurster, S., Buzengeiger, J., Meyer, J., Kasper, G., 2014. Pressure drop and liquid transport thruogh coalescence filter media used for oil mist filtration. Int. J. Multiphase Flow. 58, 313-324.

Kampa, D., Wurster, S., Meyer, J., Kasper, G., 2015. Validation of a new phenomenological "jump-and-channel" model for the wet pressure drop of oil mist filters. Chem. Eng. Sci., 122, 150-160.

Keusen, G., 2003. Anwendung der Streulicht-Partikelgrößen-Zählanalyse zur Charakterisierung von Tropfenkollektiven bei der Dieselöl-Hochdruckzerstäubung. Chemical and Process Engineering. Karlsruhe, Universität Karlsruhe. Doctor of Engineering.

Knutson, E. O., Whitby, K. T., 1975. Accurate measurements of aerosol electric mobility moments. J. Aerosol Sci. 6, 453-460. May, K. R., 1950. The measurement of airborne droplets by the magnesium oxide method. J. Sci. Instrum. 27, 128-130.

May, K. R., 1950. The measurement of airborne droplets by the magnesium oxide method. J. Sci. Instrum. 27, 128-130.

Mullins, B. J., Braddock, R.D., Agranovski, I. E., Cropp, R.A. and O'Leary, R. A., 2005. Observation and modeling of clamshell droplets on vertical fibres subjected to gravitational and drag forces, J. Colloid Interface Sci., 284, 245-254.

Mullins B. J., Pfrang A., Braddock R. D., Schimmel T. and Kasper G., 2007. Detachment of liquid droplets from fibres - Experimental and theoretical evaluation of detachment force due to interfacial tension effects. J. Colloid Interface Sci. 312, 333 - 340.

Mullins, B. J., Mead-Hunter, R., Pitta, R. N., Kasper, G., Heikamp, W., 2014. Comparative performance of philic and phobic oil-mist filters. AIChE J. 60, 2976-2984.

Newitt, D., 1954. Liquid entrainment – 1. The mechanism of drop formation from gas or vapour bubbles. Trans. Instn Chem. Engrs. 32, 244-261.

Preining, O., 1983. Optical single-particle counters to obtain the spatial inhomogeneity of particulate clouds. J. Aerosol Sci. 2, 79-90.

Raynor, P. C., Leith, D., 2000. The influence of accumulated liquid on fibrous filter performance. J. Aerosol Sci. 31, 19-34.

Resch F. J., Darrozes J. S. and Afeti G. M., 1986. Marine liquid aerosol production from bursting bubbles. J. Geophys. Res. 91, 1019.

Stone, H. A., 1994. Dynamics of drop deformation and breakup in viscous fluids. Annu. Rev. Fluid Mech. 26, 65-102.

Umhauer, H., Meyer, J., Schiel, A., 2008. A novel device for single particle light scattering size analysis and concentration measurement at high pressures and temperatures. Part. Part. Syst. Char. 25, 119-135.

Wurster S., Kampa D., Meyer J., Mullins B. J. and Kasper G., 2012. First measurements of large drop re-entrainment from an oil-mist filter. WFC11, Graz.

Wurster, S., Kampa, D., Meyer, J., Müller, T., Mullins, B. J. and Kasper, G., 2015a. Measurement of oil entrainment rates and drop size spectra from coalescence filter media, Chem. Eng. Sci. 132, 72-80.

Wurster, S., Meyer, J., Kolb, H. E. and Kasper, G., 2015b. Bubbling vs. Blow-off – On the relevant mechanism(s) of drop entrainment from oil mist filter media, Sep. Purif. Technol. 152, 70-79.